SSCL-610

SSCL-610
January 1993
Distribution Category: 414

G. Dugan

Interpretation of Photo-desorption Data in a Diffusion Model and Application To Candidate SSC Beam Tube Surfaces

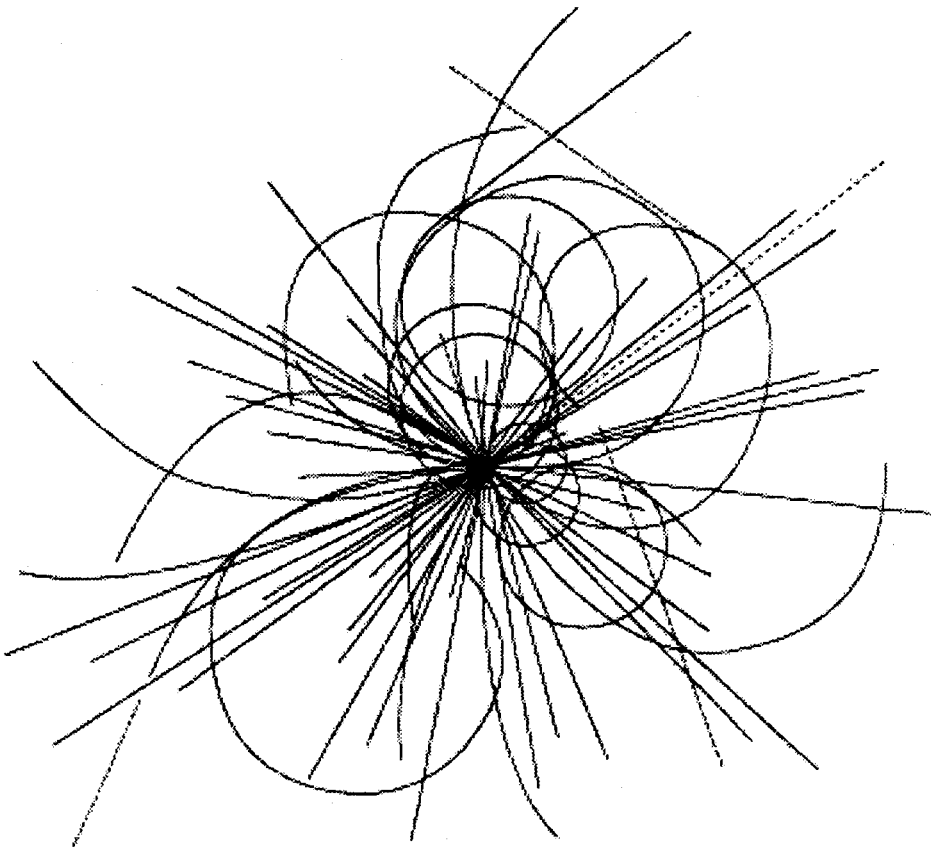

Superconducting Super Collider Laboratory

SSCL-610

Interpretation of Photodesorption Data in a Diffusion Model and Application To Candidate SSC Beam Tube Surfaces

G. Dugan

Superconducting Super Collider Laboratory*
2550 Beckleymeade Ave.
Dallas, TX 75237

January 1993

*Operated by the Universities Research Association, Inc., for the U.S. Department of Energy under Contract No. DE–AC35–89ER40486.

1.0 INTRODUCTION

In this paper, a diffusion model is developed as a phenomenological description of the photodesorption process. The model starts from the work described in References 1 and 2. Expressions are derived for the dependence of the photodesorption coefficients on certain semi-phenomenological parameters. Photodesorption data for possible Superconducting Super Collider (SSC) beam tube surfaces are fitted to the derived form, and values for the parameters are extracted from the fits.

In an application to the vacuum problem for the SSC, the time required to desorb a monolayer is derived as a function of the model parameters. The range of parameter space required for long monolayer desorption times (up to 4000 hrs) is established, and this is compared with the values of the parameters obtained from the fits to photodesorption data discussed above. The sensitivity of the results to various model assumptions is also explored.

2.0 DERIVATION OF EXPRESSIONS

One of the principal features of the process of photodesorption is the "clean-up" phenomenon. The photodesorption coefficient, η, is defined as follows:

$$\eta = \Phi/\dot{\gamma}. \tag{1}$$

In this definition, Φ is the flux of photodesorbed molecules (in molecules/cm^2/sec) and $\dot{\gamma}$ is the incident flux in photons/cm^2/sec. It is found experimentally that η is a monotonically decreasing function of the integrated incident particle flux Γ, where

$$\Gamma = \int \dot{\gamma} dt. \tag{2}$$

The reduction in η with incident integrated flux is referred to as "clean-up" of the surface.

In the diffusion model, the overall process of photodesorption is described in terms of the liberation of molecules directly from the surface into the vacuum due to the incident photon flux, together with transport of additional molecules from the volume of the material to the depleted surface by a process of diffusion.

The direct photo-stimulated liberation of molecules from the material can be related to the microscopic process of ejection of a gas molecule from the material by the electromagnetic interaction of the molecule with the photon. The flux of photons within the material is assumed to vary like

$$\dot{\gamma}(x) = \dot{\gamma} \ \mathrm{Exp}\left(\frac{-x}{\lambda_T}\right), \tag{3}$$

where x is the depth in the material, and the characteristic length is given by

$$\frac{1}{\lambda_T} = \varrho\sigma_T(E). \tag{4}$$

Here $\sigma_T(E)$ is the total absorption cross section for the photons (of energy E) in the material, and ϱ is the density (in atoms/cm^3) of interacting atoms responsible for the total absorption process.

Let us designate the cross section (in cm^2/molecule) for the photodesorption process as $\sigma_D(E,M)$. Further, let $c(x,t)$ be the volume concentration (in molecules/cm^3) of gas in the bulk material. Then we have the following equation for the flux Φ of photodesorbed molecules produced at distance x in the material:

$$\begin{aligned} d\Phi(x,t) &= \dot{\gamma}(x)c(x,t)\sigma_D(E,M)\ dx \\ &= \dot{\gamma}\ \mathrm{Exp}\left(\frac{-x}{\lambda_T}\right)c(x,t)\sigma_D(E,M)\ dx. \end{aligned} \tag{5}$$

If we designate $P(x)$ as the probability that a molecule desorbed at x escapes from the material, then taking

$$P(x) = \mathrm{Exp}\left(\frac{-x}{\lambda_M}\right) \tag{6}$$

the total flux of desorbed molecules is

$$\Phi(t) = \sigma_D(E,M)\int_0^\infty \dot{\gamma}\ \mathrm{Exp}\left(\frac{-x}{\lambda}\right)c(x,t)\ dx \tag{7}$$

with

$$\frac{1}{\lambda} = \frac{1}{\lambda_M} + \frac{1}{\lambda_T}. \tag{8}$$

If we assume that the characteristic length λ is small compared to the distance over which $c(x,t)$ varies, then we have

$$\Phi(t) = \dot{\gamma}\lambda c(0,t)\sigma_D(E,M). \tag{9}$$

In terms of a phenomenological constant (units cm^3), $\varkappa$, where

$$\varkappa = \lambda \sigma_D(E, M), \tag{10}$$

we have

$$\Phi(t) = \varkappa \; c(0, t) \; \dot{\gamma}. \tag{11}$$

This equation for the molecular flux $\Phi(t)$ leaving the surface provides a boundary condition at $x = 0$ which the solution to the diffusion equation within the metal must satisfy. The diffusion equation is

$$D \; \frac{\partial^2 c(x, t)}{\partial x^2} = \frac{\partial c(x, t)}{\partial t} \tag{12}$$

and the boundary condition is

$$\Phi(t) = D \; \frac{\partial c(0, t)}{\partial x} = \varkappa \; c(0, t) \; \dot{\gamma}. \tag{13}$$

As an initial condition, the concentration as a function of x must be specified at $t = 0$. The case of a localized concentration near the surface may be modeled as an exponentially varying function:

$$c(x, 0) = c_0 \; \mathrm{Exp}(-x\Lambda). \tag{14}$$

In this equation, $1/\Lambda$ represents the distance over which the gas is "localized" adjacent to the metal surface. In this case, there is a finite gas load in the metal. The total gas load per unit area is

$$Q = \int_0^\infty c(x, 0) dx = \frac{c_0}{\Lambda}. \tag{15}$$

The solution to the differential Eq. (12), subject to the boundary condition Eq. (13), and initial condition, Eq. (14), may be obtained by the method of Laplace transforms.[3] The Laplace transform is defined as

$$\tilde{c}(x,p) = \int_0^\infty \mathrm{Exp}(-pt)c(x,t)\ dt. \tag{16}$$

This transformation is applied to the differential equation (12):

$$\int_0^\infty \mathrm{Exp}(-pt)\ D\frac{\partial^2 c(x,t)}{\partial x^2}dt = D\frac{\partial^2 \tilde{c}(x,p)}{\partial x^2} = \int_0^\infty \mathrm{Exp}(-pt)\frac{\partial c(x,t)}{\partial t}dt \tag{17}$$

$$= p\tilde{c}(x,p) - c(x,0).$$

Here $c(x,0)$ is the initial condition. The transformed boundary condition is

$$D\frac{\partial \tilde{c}(0,p)}{\partial x} = \varkappa\ \tilde{c}(0,p)\ \dot{\gamma}. \tag{18}$$

Subject to this boundary condition, then, the transformed ordinary differential equation,

$$D\frac{\partial^2 \tilde{c}(x,p)}{\partial x^2} = p\tilde{c}(x,p) - c(x,0) \tag{19}$$

is solved for the quantity $\tilde{c}(x,p)$. Then, the result is inverse Laplace transformed to obtain $c(x,t)$.

To simplify the result, we introduce the following quantities with the units of time:

$$\tau = \frac{D}{(\varkappa\dot{\gamma})^2}, \tag{20}$$

$$\tau_p = \frac{1}{\Lambda^2 D} \tag{21}$$

and a quantity with the units of distance,

$$h = \sqrt{D\tau} = \frac{D}{\varkappa\dot{\gamma}}. \tag{22}$$

The solution to Eq. (12) for the concentration density is,

$$\frac{c(x,t)}{c_0} = \frac{\left[\begin{array}{c} \mathrm{Exp}(t/\tau_p)\left(\sqrt{\tau} - \sqrt{\tau_p}\right)\ \mathrm{Erfc}\left[\sqrt{\frac{t}{\tau_p}}\frac{x}{2h}\sqrt{\frac{\tau}{t}}\right] \\ -\ 2\mathrm{Exp}\left(\frac{t}{\tau} + \frac{x}{h} + x\Lambda\right)\sqrt{\tau_p}\,\mathrm{Erfc}\left[\sqrt{\frac{t}{\tau}} + \frac{x}{2h}\sqrt{\frac{\tau}{t}}\right] \\ +\ \mathrm{Exp}\left(\frac{t}{\tau_p} + 2x\Lambda\right)\left(\sqrt{\tau} + \sqrt{\tau_p}\right)\mathrm{Erfc}\left[\sqrt{\frac{t}{\tau_p}} + \frac{x}{2h}\sqrt{\frac{\tau}{t}}\right] \end{array}\right]}{2\mathrm{Exp}(x\Lambda)\left(\sqrt{\tau} - \sqrt{\tau_p}\right)}. \tag{23}$$

The concentration at the surface is given by

$$\frac{c(0,t)}{c_0} = \frac{\mathrm{Exp}(t/\tau_p)\sqrt{\tau}\,\mathrm{Erfc}\left[\sqrt{\frac{t}{\tau_p}}\right] - \mathrm{Exp}\left(\frac{t}{\tau}\right)\sqrt{\tau_p}\,\mathrm{Erfc}\left[\sqrt{\frac{t}{\tau}}\right]}{\left(\sqrt{\tau} - \sqrt{\tau_p}\right)}. \tag{24}$$

In the case of an initial concentration density which is uniform in the volume of the metal (*i.e.*, $c(0,t) = c_0$), the above solutions apply in the limits $\Lambda \to 0$ ($\tau_p \to \infty$). The concentration density is

$$\frac{c(x,t)}{c_0} = \mathrm{Erf}\left[\frac{x}{2h}\sqrt{\frac{\tau}{t}}\right] + \mathrm{Exp}\left(\frac{t}{\tau} + \frac{x}{h}\right)\mathrm{Erfc}\left[\sqrt{\frac{t}{\tau}} + \frac{x}{2h}\sqrt{\frac{\tau}{t}}\right] \tag{25}$$

and the concentration at the surface is

$$\frac{c(0,t)}{c_0} = \mathrm{Exp}\left(\frac{t}{\tau}\right)\mathrm{Erfc}\left[\sqrt{\frac{t}{\tau}}\right]. \tag{26}$$

The total gas/area evolved from the surface at time t, $m(t)$, is given by

$$m(t) = \int_0^t \Phi(t')dt' = \varkappa\dot{\gamma} \int_0^t c(0,t')dt'. \tag{27}$$

For the case of the concentration at the surface given by Eq. (24), we have

$$\frac{m(t)}{c_0} = \varkappa\dot{\gamma}\sqrt{\tau\tau_p}\left[1 - \frac{\mathrm{Exp}\left(\frac{t}{\tau}\right)\sqrt{\tau}\,\mathrm{Erfc}\left[\sqrt{\frac{t}{\tau}}\right] - \mathrm{Exp}\left(\frac{t}{\tau_p}\right)\sqrt{\tau_p}\,\mathrm{Erfc}\left[\sqrt{\frac{t}{\tau_p}}\right]}{\sqrt{\tau} - \sqrt{\tau_p}}\right] \tag{28}$$

while for the concentration at the surface given by Eq. (26), we have

$$\frac{m(t)}{c_0} = \varkappa\dot{\gamma}\sqrt{\tau}\left(2\sqrt{\frac{t}{\pi}} - \sqrt{\tau} + \mathrm{Exp}\left(\frac{t}{\tau}\right)\sqrt{\tau}\,\mathrm{Erfc}\left[\sqrt{\frac{t}{\tau}}\right]\right) . \tag{29}$$

The limit of Eq. (28) as $t \rightarrow \infty$ is the total gas load Q as given by Eq. (15). The limit of Eq. (29) as $t \rightarrow \infty$ is, of course, infinite.

Given these expressions, the photodesorption coefficient of Eq. (1) can be written as

$$\begin{aligned} \eta(t) &= \Phi(t)/\dot{\gamma} \\ &= \varkappa\ c(0,t) \end{aligned} \tag{30}$$

which becomes, upon substitution from Eq. (24),

$$\begin{aligned} \frac{\eta(t)}{\varkappa c_0} &= \frac{\mathrm{Exp}(t/\tau_p)\sqrt{\tau}\,\mathrm{Erfc}\left[\sqrt{\frac{t}{\tau_p}}\right] - \mathrm{Exp}\left(\frac{t}{\tau}\right)\sqrt{\tau_p}\,\mathrm{Erfc}\left[\sqrt{\frac{t}{\tau}}\right]}{\left(\sqrt{\tau} - \sqrt{\tau_p}\right)} \\ &= \frac{\mathrm{Exp}\left(\frac{t}{\tau}\right)\mathrm{Erfc}\left[\sqrt{\frac{t}{\tau}}\right] - \mathrm{Exp}\left(\frac{t}{\tau}\frac{\tau}{\tau_p}\right)\sqrt{\frac{\tau}{\tau_p}}\,\mathrm{Erfc}\left[\sqrt{\frac{t}{\tau}\frac{\tau}{\tau_p}}\right]}{\left(1 - \sqrt{\frac{\tau}{\tau_p}}\right)} \end{aligned} \tag{31}$$

or, in the case of a uniform initial concentration, using Eq. (26),

$$\frac{\eta(t)}{\varkappa c_0} = \mathrm{Exp}\left(\frac{t}{\tau}\right)\mathrm{Erfc}\left[\sqrt{\frac{t}{\tau}}\right]. \tag{32}$$

The photodesorption coefficient is typically expressed as a function of the integrated flux Γ, given by Eq. (2). In the case of $\dot{\gamma}$ which is constant in time, then

$$\Gamma = \dot{\gamma}t. \tag{33}$$

Let us define the parameters p_1, p_2, and p_3 as follows:

$$p_1 = \mathrm{Log}_{10}(\varkappa c_0), \qquad p_2 = \sqrt{\frac{\Gamma_0}{\tau\dot{\gamma}}}, \qquad p_3 = \sqrt{\frac{\tau}{\tau_p}}. \tag{34}$$

Note that all these parameters are dimensionless. Then we have the following for Eqs. (29) and (31), respectively, in terms of these parameters:

$$\frac{\eta(\chi)}{10^{p_1}} = \frac{\mathrm{Exp}(p_2{}^2\chi)\mathrm{Erfc}\left[p_2\sqrt{\chi}\right] - \mathrm{Exp}(p_2{}^2p_3{}^2\chi)p_3\mathrm{Erfc}\left[p_2p_3\sqrt{\chi}\right]}{(1 - p_3)}, \tag{35}$$

$$\frac{\eta(\chi)}{10^{p_1}} = \mathrm{Exp}\left(p_2{}^2\chi\right)\mathrm{Erfc}\left[p_2\sqrt{\chi}\right] \ . \tag{36}$$

In these equations, $\chi = \Gamma/\Gamma_0$. Γ_0 is simply a scaling factor used to define the scaled integrated flux, χ. Substituting for τ and τ_p from Eqs. (20) and (21) into Eq. (34), we can solve Eqs. (34) for the fundamental quantities $\varkappa$, c_0 and Λ in terms of the dimensionless parameters, with the following results:

$$\varkappa = p_2\sqrt{\frac{D}{\Gamma_0\dot{\gamma}}}, \tag{37}$$

$$c_0 = \frac{10^{p_1}}{p_2}\sqrt{\frac{\Gamma_0\dot{\gamma}}{D}}, \tag{38}$$

$$\Lambda = p_2p_3\sqrt{\frac{\dot{\gamma}}{D\Gamma_0}}. \tag{39}$$

3.0 RESULTS OF FITS

Photodesorption data for seven measurement sets have been fit to Eq. (36). A fit to Eq. (35) was also attempted, and is reported below unless the fit indicated a (nonphysical) negative value for p_3. The fit to Eq. (35) indicated positive values for p_3 for data sets 1,5,6 and 7. In Table 1, the data sets are defined.

TABLE 1. DATA SET DEFINITIONS.

DATA SET INDEX	MATERIAL	TREATMENT	TEST LOCALE	REFERENCE
1	OHFC Cu	CERN cleaning; in-situ bake	DCI	4
2	Electrodeposited Cu on SS	Unknown	BNL	5
3	Electrodeposited Cu on SS	BNL cleaning	BNL	6
4	OFHC Cu	CERN cleaning	DCI	7
5	Electrodeposited Cu on SS	BNL cleaning	BINP	8
6	Electrodeposited Cu on SS	BNL cleaning	BINP	9
7	Electrodeposited Cu on SS	BNL cleaning	BNL	10

The photodesorption data analyzed here were all data taken in long tubes. For such data, the results are generally given by presenting the photodesorption coefficient η as a function of the linear incident photon density in the tube (ζ, in photons/length). The model discussed above treats the photodesorption coefficient as a function of the integrated photon flux Γ (in photons/area). To relate these two quantities, we write

$$\Gamma = \zeta/w, \tag{40}$$

where w is the effective circumferential distance in the tube over which the photodesorption process occurs. In this analysis, we have taken $w = \pi d$, where d is the tube diameter. This is done under the assumption that, either as a result of photon scattering in the tube, or through the process of photoelectron production followed by subsequent electrodesorption, the entire tube circumference is involved uniformly in the desorption process. With this assumption, the scaling parameter is $\chi = \Gamma/\Gamma_0 = \zeta/\zeta_0$, with ζ_0 10^{16} photons/cm. Thus a linear photon flux of 10^{18} photons/meter corresponds to $\chi = 1$.

The fits to the seven data sets are illustrated in Figures 1–7. These are log-log plots in which the abscissa is $\log_{10}\eta$, and the ordinate is $\log_{10}\chi$. The points represent the data; the errors on all data points have been (arbitrarily) taken to be 0.1 in $\log_{10}\eta$. This error has also been used to calculate the errors in the fitted and derived parameters, using standard error propagation formulae. In Figures 1–7, the dotted line represents the fitted 2-parameter function, Eq. (36), and the solid line represents the 3-parameter function, Eq. (35). In Tables 2 and 3, the values of the fit parameters are given.

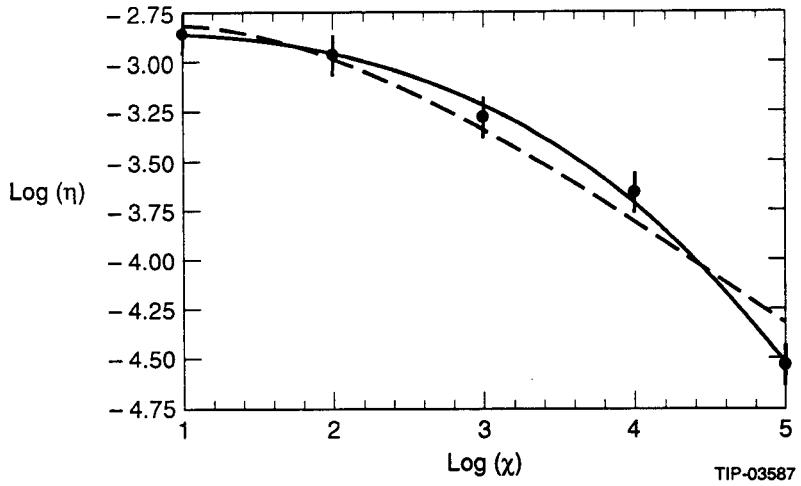

Figure 1. Data Set 1.

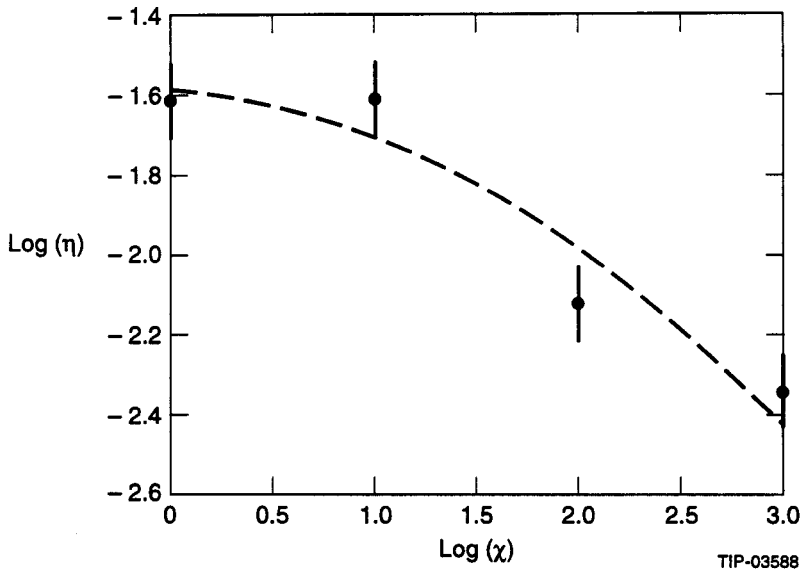

Figure 2. Data Set 2.

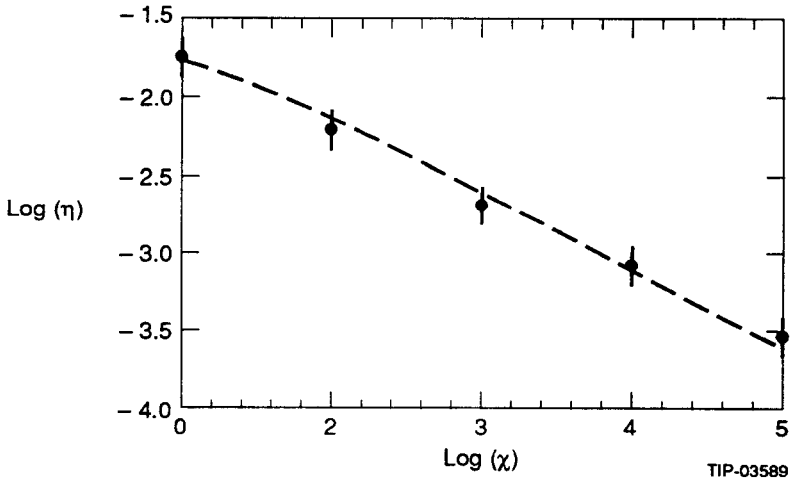

Figure 3. Data Set 3.

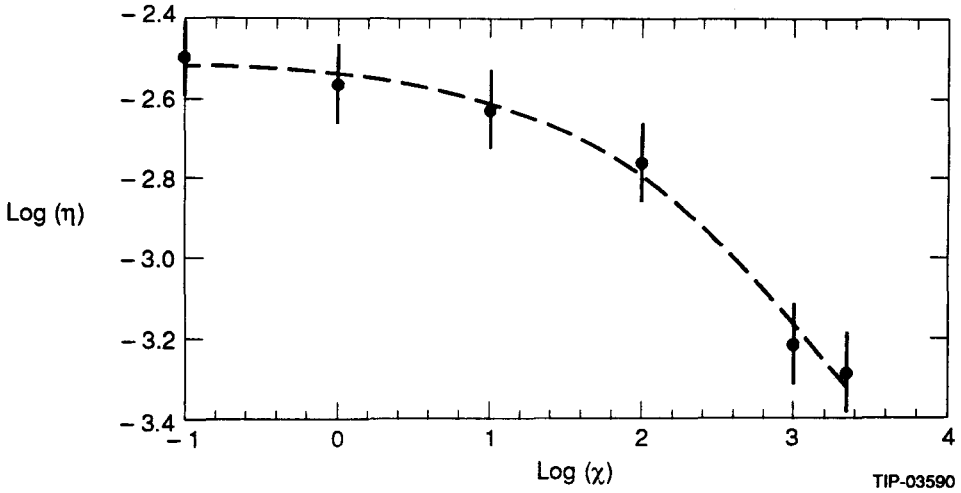

Figure 4. Data Set 4.

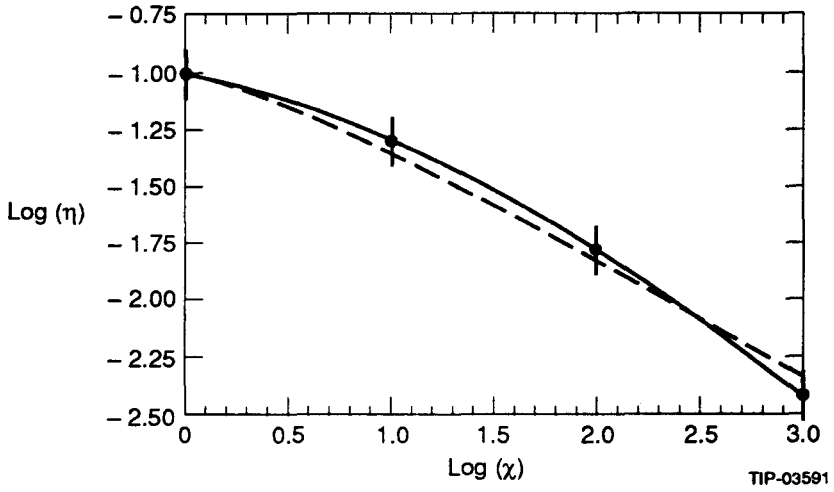

Figure 5. Data Set 5.

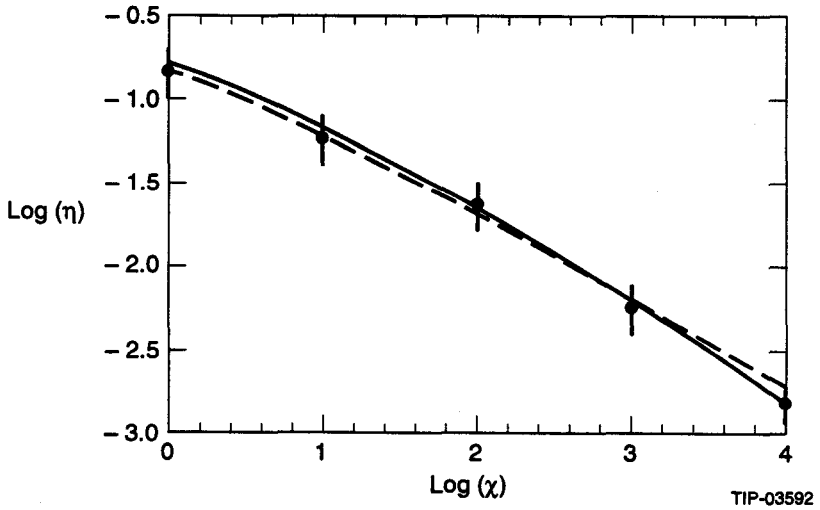

Figure 6. Data Set 6.

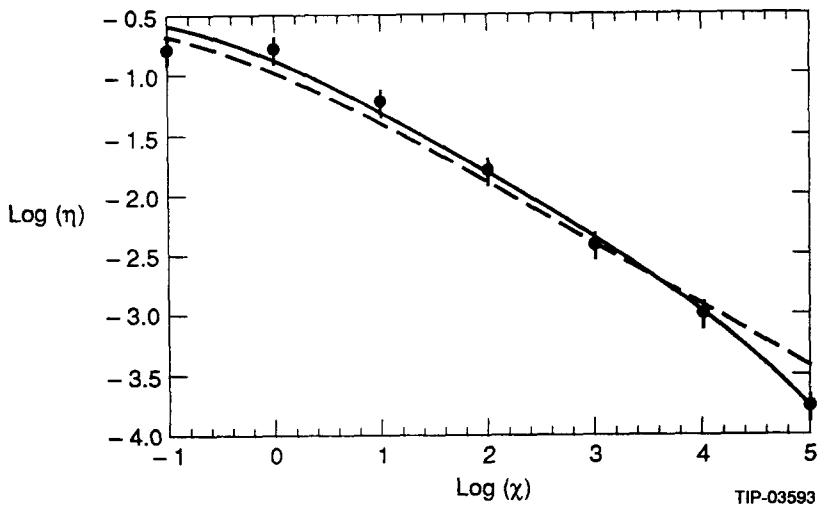

Figure 7. Data Set 7.

TABLE 2. RESULTS OF 2 PARAMETER FITS.

DATA SET INDEX	p_1	δp_1	p_2	δp_2
1	−2.705	0.111	0.07144	0.0233
2	−1.526	0.103	0.1365	0.0517
3	−1.449	0.2628	0.2609	0.1748
4	−2.503	0.0649	0.0746	0.0194
5	−0.669	0.2434	0.8166	0.5203
6	−0.4502	0.2907	1.0136	0.7363
7	−0.4826	0.1397	1.51	0.5347

TABLE 3. RESULTS OF 3 PARAMETER FITS.

DATA SET INDEX	p_1	δp_1	p_2	δp_2	p_3	δp_3
1	−2.811	0.100	0.03078	0.0161	0.07696	0.0813
5	−0.802	0.196	0.456	0.315	0.0210	0.0331
6	−0.461	0.330	0.859	0.774	0.00270	0.0044
7	−0.3925	0.335	1.466	1.3725	0.00151	0.00186

In order to calculate the derived parameters defined in Eqs. (37) to (39), the photon flux must be known. For each data set, the photon flux $\dot{\gamma}$, in photons/cm^2/sec, has been estimated using the following equation:

$$\dot{\gamma} = 1.28 \times 10^{14} \frac{IE\theta}{lw}, \tag{41}$$

where I is the storage ring beam current in mA, E is the beam energy in GeV, θ is the horizontal acceptance angle in mrad, l is the length of the tube in cm, and $w = \pi d$ (d = tube diameter). The results are shown in Table 4.

TABLE 4. PHOTON FLUX ESTIMATES.

DATA SET INDEX	E	i	θ	l	w	$\dot{\gamma}$
UNITS	GeV	mA	mrad	cm	cm	10^{13}/cm^2/sec
1	1.72	150	5.0	300	41.0	1.33
2	0.75	150	3.4	300	10.4	1.57
3	0.75	150	3.4	300	9.4	1.73
4	1.72	150	5.0	300	41.0	1.33
5	0 .54	200	0.55	100	10.4	0.733
6	0 .54	200	4.2	100	10.4	5.6
7	0.75	800	2.1	100	10.4	15.5

Given the value of $\dot{\gamma}$, and given the scale factor $\Gamma_0 = \zeta_0/w$ from Eq. (40), Eqs. (37)–(39) relate the four derived parameters $\varkappa$, c_0, D, and Λ to the three fitted parameters p_1, p_2, and p_3. We must thus determine one of the derived parameters from some other source. We choose to fix the value of the diffusion constant, D. Previous similar studies of diffusion-modeled photo- and electrodesorption[1,2,11,12] have obtained values for D which range from 10^{-19} to 7×10^{-18} cm^2/sec. We will fix D at a representative number, $D = 5 \times 10^{-18}$ cm^2/sec, for all the data sets. Then, using Eqs. (37)–(39), we convert the fit parameters p_1, p_2, and p_3 into the derived quantities $\varkappa$, c_0 and Λ. The parameters τ, τ_p, and h have also been calculated. The results are shown in Tables 5, 6a and 6b.

Also included in Table 6b are the parameters r and m_1. The parameter r is the ratio

$$r = \tau/\tau_p. \tag{42}$$

This will be discussed further in the next section. The quantity m_1 is the total number of monolayers of gas in the bulk; it is calculated as

$$m_1 = \frac{Q}{m_0} = \frac{c_0}{\Lambda m_0} \tag{43}$$

in which m_0 is the monolayer surface concentration, which is taken as $m_0 = 6 \times 10^{15}$/cm^2.

TABLE 5. DERIVED PARAMETERS, 2 PARAMETER FITS.

DATA SET INDEX	$\varkappa$	$\delta\varkappa$	Log c_0	δLog c_0	c_0	τ	h
UNITS	10^{-24} cm^3	10^{-24} cm^3	cm^{-3}	cm^{-3}	10^{21} cm^{-3}	sec	Å
1	2.80	0.91	20.84	0.06	0.703	3559	13.4
2	2.47	0.94	22.08	0.09	12.02	3288	12.8
3	4.30	2.88	21.9172	0.055	8.26	900	6.72
4	2.93	0.76	21.03	0.074	1.074	3263	12.8
5	21.7	13.8	21.99	0.063	9.87	197	3.14
6	9.75	7.08	22.56	0.053	36.4	16.7	0.91
7	8.72	3.08	22.57	0.042	37.7	2.7	0.37

TABLE 6A. DERIVED PARAMETERS, 3 PARAMETER FITS.

DATA SET INDEX	$\varkappa$	$\delta\varkappa$	Log c_0	δLog c_0	c_0	$1/\Lambda$	$\delta(1/\Lambda)$	τ	h
UNITS	10^{-24}cm^3	10^{-24}cm^3	cm^{-3}	cm^{-3}	10^{21}cm^{-3}	Å	Å	sec	Å
1	1.207	0.631	21.107	0.156	1.28	402	233	19 179	30.96
5	12.1	8.4	22.11	0.135	13.01	267	265	632	5.62
6	8.27	7.45	22.62	0.087	41.78	399	372	23	1.07
7	8.46	7.92	22.68	0.087	47.86	250	97	2.9	0.38

TABLE 6B. DERIVED PARAMETERS, 3 PARAMETER FITS.

DATA SET INDEX	τ	τ_p	r	m_1
UNITS	sec	10^6 sec	10^{-4}	
1	19 179	3.24	59.2	0.86
5	632	1.43	4.41	5.8
6	23	3.19	0.072	27.8
7	2.9	1.26	0.023	20.0

4.0 INTERPRETATION OF THE MODEL EQUATIONS AND PARAMETERS

The model equations given above may be conveniently rewritten in terms of scaled time and distance variables. The scaled time variables to be used will be $\psi = t/\tau$; and $r\psi = t/\tau_p$, where

$$r = \frac{\tau}{\tau_p} = \left[\frac{\Lambda D}{\varkappa\dot{\gamma}}\right]^2 = [\Lambda h]^2. \tag{44}$$

The scaled distance variables will be $\xi = x/h$, and $\sqrt{r}\xi = x\Lambda$. In terms of these variables, we have, for the case of an initially uniform concentration density, the following equations derived respectively from Eqs. (25), (32) and (29):

$$\frac{c(\xi,\psi)}{c_0} = \mathrm{Erf}\left(\frac{\xi}{2\sqrt{\psi}}\right) + \mathrm{Exp}(\xi + \psi)\mathrm{Erfc}\left(\sqrt{\psi} + \frac{\xi}{2\sqrt{\psi}}\right) \tag{45}$$

$$\frac{\eta(\psi)}{\varkappa c_0} = \mathrm{Exp}(\psi)\mathrm{Erfc}\left(\sqrt{\psi}\right) \tag{46}$$

$$\frac{m(\psi)}{\left[\frac{c_0 D}{\varkappa\gamma}\right]} = 2\sqrt{\frac{\psi}{\pi}} - 1 + \mathrm{Exp}(\psi)\mathrm{Erfc}\left(\sqrt{\psi}\right). \tag{47}$$

Similarly, for Eqs. (23), (31) and (28), we have in the scaled variables,

$$\frac{c(\xi,\psi)}{c_0} = \frac{\left[\begin{array}{l}\mathrm{Exp}\left(\sqrt{r}\xi + r\psi\right)\mathrm{Erfc}\left(\sqrt{r\psi} + \frac{\xi}{2\sqrt{\psi}}\right)\left(\sqrt{r} + 1\right) \\ \quad + \mathrm{Exp}(r\psi)\mathrm{Erfc}\left(\sqrt{r\psi} - \frac{\xi}{2\sqrt{\psi}}\right)\left(\sqrt{r} - 1\right) \\ - 2\mathrm{Exp}\left(\psi + \left(1 + \sqrt{r}\right)\xi\right)\mathrm{Erfc}\left(\sqrt{\psi} + \frac{\xi}{2\sqrt{\psi}}\right)\end{array}\right]}{2\mathrm{Exp}\left(\sqrt{r}\xi\right)\left(\sqrt{r} - 1\right)}, \tag{48}$$

$$\frac{\eta(\psi)}{\varkappa c_0} = \frac{\mathrm{Exp}(\psi)\mathrm{Erfc}\left(\sqrt{\psi}\right) - \sqrt{r}\,\mathrm{Exp}(r\psi)\mathrm{Erfc}\left(\sqrt{r\psi}\right)}{1 - \sqrt{r}}, \tag{49}$$

$$\frac{m(\psi)}{\left[\frac{c_0 D}{\varkappa\gamma}\right]} = \frac{1}{\sqrt{r}} - \frac{\mathrm{Exp}(\psi)\mathrm{Erfc}\left(\sqrt{\psi}\right) - \frac{\mathrm{Exp}(r\psi)\mathrm{Erfc}\left(\sqrt{r\psi}\right)}{\sqrt{r}}}{\sqrt{r} - 1}. \tag{50}$$

The scaled concentration density, $\frac{c(\xi,\psi)}{c_0}$, from Eq. (45), is plotted as a function of ξ for several values of $\mathrm{Log}_{10}\psi$, in Figure 8.

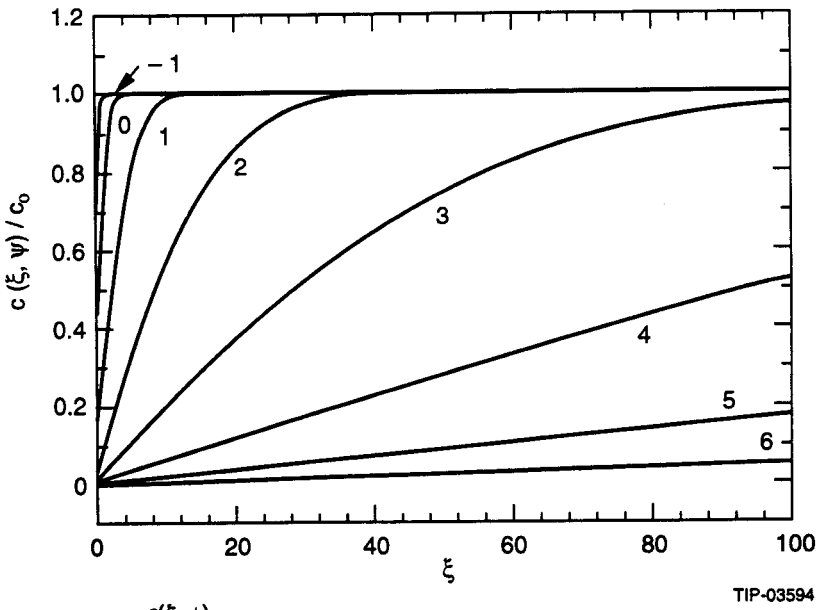

Figure 8. $\frac{c(\xi,\psi)}{c_0}$ vs. ξ, from Eq. (45). The Curves are Labeled by $\mathrm{Log}_{10}\psi$.

The scaled concentration density shows the characteristic behavior of the solution to a diffusion equation. The general relation between distance and time $x^2 \cong 4Dt$, becomes, in the scaled variables, $\xi^2 \cong 4\psi$. As Figure 8 shows, the distance over which the scaled density varies, in ξ, is roughly given by $2\sqrt{\psi}$. The distance scale parameter, h, as given by Eq. (22), is inversely related to the product $\varkappa\gamma$. Thus, as either the photon flux increases, or the effective photodesorption cross section increases, the scale parameter shrinks: the region over which the concentration density is depleted, and over which the density gradient is large, tends to be confined closer to the surface.

The scaled concentration density, $\frac{c(\xi,\psi)}{c_0}$, from Eq. (48), for the specific case of $\mathrm{Log}_{10}\, r = -4$, is plotted as a function of ξ for several values of $\mathrm{Log}_{10}\psi$, in Figure 9.

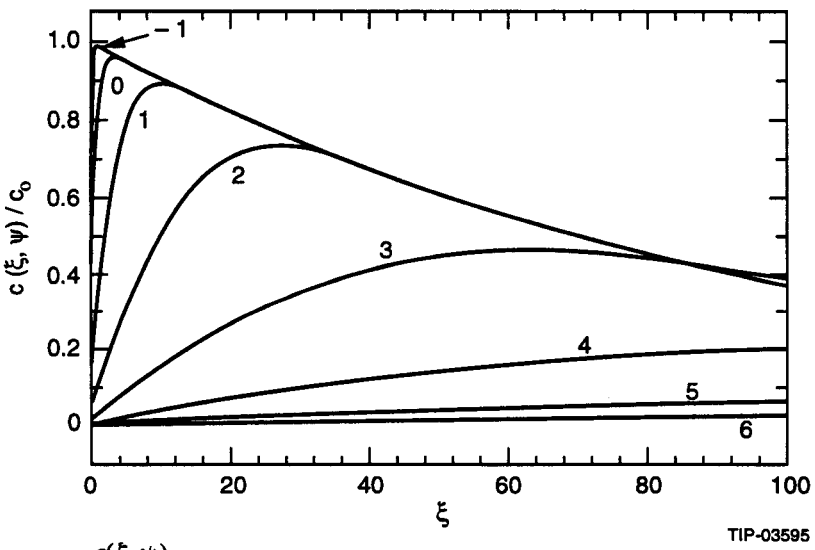

Figure 9. $\frac{c(\xi,\psi)}{c_0}$ vs. ξ, from Eq. (48), for $r = 10^{-4}$. The Curves are Labeled by $\mathrm{Log}_{10}\psi$.

We see the same general behavior here, except that the initial distribution is exponential. The parameter $1/\Lambda$ is a measure of the distance over which the initial density varies. The physical interpretation of the time τ_p is related to this distance $1/\Lambda$. Since $1/\Lambda^2 = D\tau_p$, we may interpret τ_p as the characteristic time scale at which the exponential nature of the initial distribution will be important in the problem. It is only at times $t \geq \tau_p$ that the effect of the exponential falloff in the initial concentration density will be evident at the surface of the metal.

This can be seen in the form of the scaled photodesorption function, Eq. (49). This function, $\frac{\eta(\psi)}{\varkappa c_0}$, is plotted vs. ψ for several values of $\mathrm{Log}_{10} r$, in Figure 10.

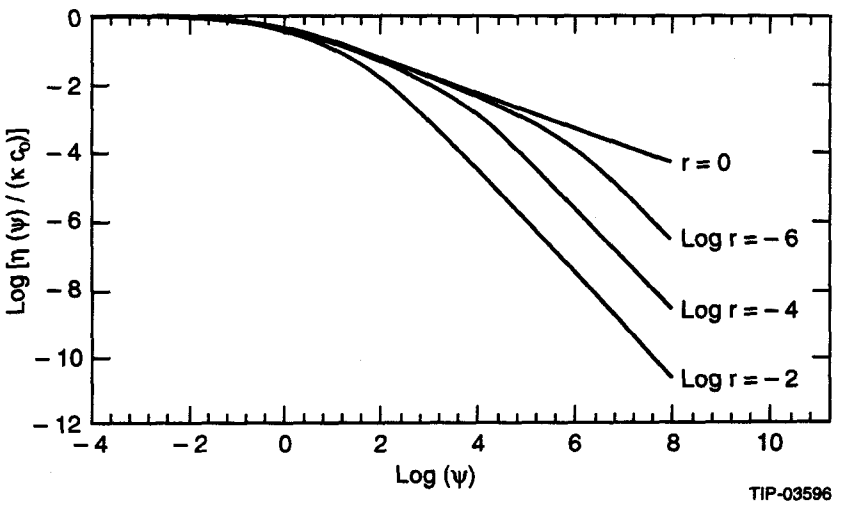

Figure 10. $\frac{\eta(\psi)}{\varkappa c_0}$, from Eq. (49), vs. ψ, for Several Values of r.

Figure 10 shows that for large values of ψ, the photodesorption coefficient falls off more rapidly for finite r than for $r = 0$. Consequently, the slope on the log-log plot is also greater, typically for those values of ψ for which $r\psi \gg 1$. This behavior can be understood simply from the asymptotic limit of the expressions given above for $\frac{\eta(\psi)}{\varkappa c_0}$. The asymptotic limit is found using the following general relation, valid for $z \gg 1$,

$$\sqrt{\pi}\, z\mathrm{Exp}(z^2)\mathrm{Erfc}(z) \rightarrow 1 - \frac{1}{2z^2} + \frac{3}{4z^4} + \ldots \quad . \tag{51}$$

Using this relation, in the limit $\psi \gg 1$, Eq. (46) has the asymptotic form,

$$\frac{\eta(\psi)}{\varkappa c_0} \rightarrow \frac{1}{\sqrt{\pi\psi}} - \frac{1}{2\sqrt{\pi\psi^3}} \quad . \tag{52}$$

This implies a $t^{-(1/2)}$ dependence at large times, which gives a slope of –0.5 on a log-log plot. In the limit $\psi \gg 1$ and $r\psi \gg 1$, but $r \ll 1$, Eq. (49) has the asymptotic form

$$\frac{\eta(\psi)}{\varkappa c_0} \rightarrow \left[\frac{1}{1-\sqrt{r}}\right]\left[\frac{\left(\frac{1}{r}-1\right)}{2\sqrt{\pi\psi^3}} + \frac{3\left(1-\frac{1}{r^2}\right)}{4\sqrt{\pi\psi^5}}\right] . \tag{53}$$

This will give a $t^{-(3/2)}$ dependence at large times, and a slope of –1.5 on a log-log plot, as illustrated in Figure 10.

The scaled total gas/area evolved during the photodesorption process, $\frac{m(\psi)}{\left[\frac{c_0 D}{\varkappa\gamma}\right]}$, given in Eq. (50), is plotted in Figure 11 for several values of $\mathrm{Log}_{10}\, r$.

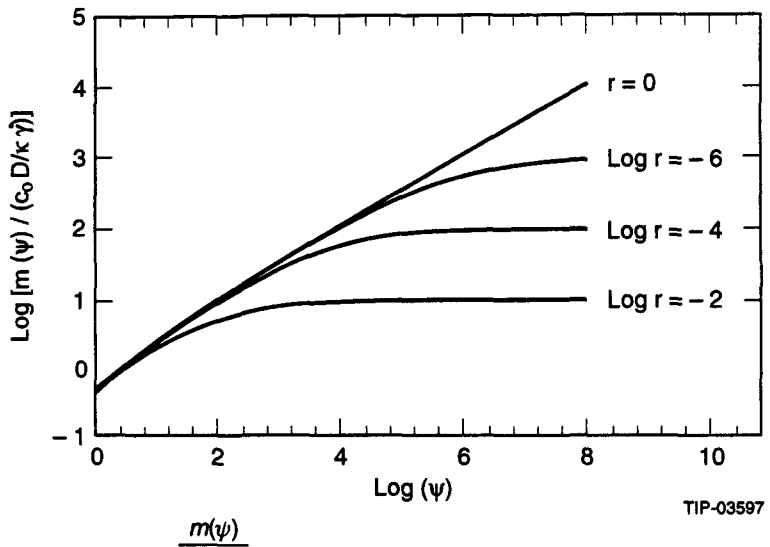

Figure 11. $\frac{m(\psi)}{\left[\frac{c_0 D}{\varkappa\gamma}\right]}$, from Eq. (49), vs. ψ, for Several Values of r.

For $r = 0$, $m(\psi)$ increases without limit, since there is an infinite gas load in the bulk of the material. For finite r, $m(\psi)$ increases to a limit. This limit is the total gas load per unit area in the bulk: the quantity Q given by Eq. (13). This general behavior, exhibited in Figure 11, can also be obtained from the asymptotic forms of Eqs. (47) and (50). Using the limiting expression given in Eq. (51), we obtain for $\psi \gg 1$ the following limit for Eq. (47):

$$\frac{m(\psi)}{\left[\frac{c_0 D}{\varkappa\gamma}\right]} \rightarrow 2\sqrt{\frac{\psi}{\pi}} + \frac{1}{\sqrt{\pi\psi}} . \tag{54}$$

This would indicate that the gas evolved/area grows like $t^{(1/2)}$ in the asymptotic limit. We can also obtain, in the limit $\psi \gg 1$ and $r\psi \gg 1$, but $r \ll 1$, the following result from Eq. (50):

$$\frac{m(\psi)}{\left[\frac{c_0 D}{\varkappa\dot{\gamma}}\right]} \rightarrow \frac{1}{\sqrt{r}} - \frac{\left(1 + \sqrt{r}\right)}{r\sqrt{\pi\psi}} \quad . \tag{55}$$

This indicates that $m(\psi)$ approaches the product

$$\left[\frac{c_0 D}{\varkappa\dot{\gamma}}\right]\frac{1}{\sqrt{r}} = \left[\frac{c_0 D}{\varkappa\dot{\gamma}}\right]\left[\frac{\varkappa\dot{\gamma}}{\Lambda D}\right] = \frac{c_0}{\Lambda} \tag{56}$$

in the above limit, as expected.

Finally, we may plot $\frac{\eta(\psi)}{\varkappa c_0}$ vs. $\frac{m(\psi)}{\left[\frac{c_0 D}{\varkappa\dot{\gamma}}\right]}$ for various values of r. The result is shown in Figure 12. For $r = 0$, in the limit $\psi \gg 1$, η varies like $\psi^{-(1/2)}$, and m varies like $\psi^{(1/2)}$, so η should vary inversely with m. A steeper-than-linear slope on a log-log plot of η vs. m would indicate that the total gas load is finite. The value of m for which η drops precipitously indicates the magnitude of the finite gas load.

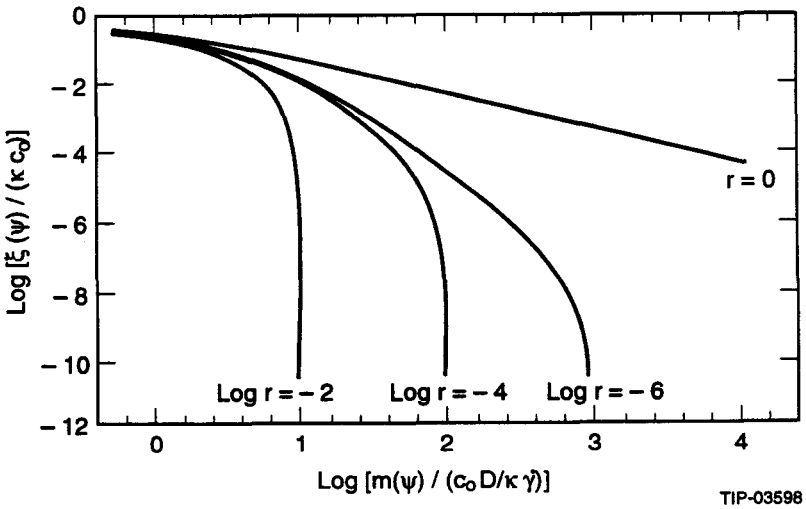

Figure 12. $\frac{\eta(\psi)}{\varkappa c_0}$ vs. $\frac{m(\psi)}{\left[\frac{c_0 D}{\varkappa\dot{\gamma}}\right]}$ for Several Values of r.

5.0 APPLICATION TO THE SSC VACUUM PROBLEM: ESTIMATE OF THE MONOLAYER FORMATION TIME

In the cold (4.2 K) bore tube of the SSC, the photodesorption process evolves gas which is rapidly frozen onto the surface of the tube. This gas accumulates as a weakly bound layer on the surface. Thermal desorption at 4 K releases gas from this layer into the cold bore vacuum; the vapor pressure of this gas in equilibrium is a function of the surface concentration of frozen gas. When the surface concentration of hydrogen gas reaches the density of a monolayer ($m_0 = 6 \times 10^{15}/\text{cm}^2$), the vapor pressure rises rapidly to a level roughly two orders of magnitude higher than that tolerable for SSC operation. When this occurs, the accelerator must be shut down and the cold bore tube warmed up to about 20 K, in order for the frozen hydrogen to evaporate and be pumped out. Since this operation represents a downtime for the accelerator, there is a lower limit requirement on the time to desorb a monolayer of hydrogen gas,which is related to the availability goals of the accelerator. The current availability budget allocates 5 hydrogen-gas warmup/pumpout cycles per year. Since the vacuum requirement which dictates this warmup is a local one, each time a piece of the accelerator's beam pipe is replaced, that piece will have to start the desorption cleanup process anew. It is currently estimated that six SSC dipoles will need to be replaced each year; each of these will require a restart of the cleanup process. The requirement of no more than five warmups/year thus sets the lower limit for the time between warmups (which equals the time to desorb a monolayer) at roughly one year. Since only time when the beam is present at full energy contributes, this lower limit is the total amount of "live time" at full energy per year, estimated to be 4000 hrs, or about 1.4×10^7 sec.

The equations developed in the preceding sections of this paper may be used to relate the time to form a monolayer (t_{mono}) to the parameters of this model. If we define $\psi_{\text{mono}} = t_{\text{mono}}/\tau$, then the inequality

$$m(\psi_{\text{mono}}) = \frac{c_0 D}{\varkappa\dot{\gamma}}\left[\frac{1}{\sqrt{r}} - \frac{\text{Exp}(\psi_{\text{mono}})\text{Erfc}\left(\sqrt{\psi_{\text{mono}}}\right) - \frac{\text{Exp}(r\psi_{\text{mono}})\text{Erfc}\left(\sqrt{r\psi_{\text{mono}}}\right)}{\sqrt{r}}}{\sqrt{r} - 1}\right] \leq m_0 \qquad (57)$$

defines the range of the model parameters which is acceptable.

5.1 $r = 0$

5.1.1 Estimate of Required c_0

For the case of $r = 0$, the expression is

$$\frac{c_0 D}{\varkappa\dot{\gamma}}\left[2\sqrt{\frac{\psi_{\text{mono}}}{\pi}} - 1 + \text{Exp}(\psi_{\text{mono}})\text{Erfc}\left(\sqrt{\psi_{\text{mono}}}\right)\right] \leq m_0 \ . \qquad (58)$$

This expression is considerably simpler in the asymptotic limit $\psi_{\text{mono}} \gg 1$. This limit implies

$$t_{\text{mono}} \gg \tau = \frac{D}{(\varkappa\dot{\gamma})^2} \ , \qquad (59)$$

or

$$\varkappa \gg \varkappa_{\min} = \sqrt{\frac{D}{t_{\text{mono}}\dot{\gamma}^2}} \quad . \tag{60}$$

For the SSC parameters $\dot{\gamma} = 10^{13}/\text{cm}^2/\text{sec}$, $t_{\text{mono}} = 1.4 \times 10^7$ sec, and $D = 5 \times 10^{-18}$ cm^2/sec, we have $\varkappa_{\min} = 6 \times 10^{-26}$ cm^3. Typical values of $\varkappa$ found in the data fits above (see Tables 5 and 6) are in the range of 10^{-24} cm^3 or greater, so this inequality is satisfied. It is thus appropriate to use the limiting form of $m(\psi)$, Eq. (54). We have that Eq. (58) becomes, to leading order in ψ_{mono},

$$m(\psi_{\text{mono}}) = \frac{c_0 D}{\varkappa\dot{\gamma}} 2 \sqrt{\frac{\psi_{\text{mono}}}{\pi}} \leq m_0 \quad . \tag{61}$$

Substituting $\psi_{\text{mono}} = t_{\text{mono}}/\tau$, and using Eq. (20) for τ, we obtain:

$$c_0 \leq \frac{m_0}{2} \sqrt{\frac{\pi}{t_{\text{mono}} D}} \quad . \tag{62}$$

Using the numerical values for m_0, t_{mono}, and D given above, this gives

$$c_0 \leq 0.6 \times 10^{21}/\text{cm}^3 \quad . \tag{63}$$

Comparing this result with the values obtained from the data, shown in Table 5, we see that the data exceeds this limit by factors ranging from 1.15 to 63. This would imply monolayer formation times smaller than t_{mono} by the square of these factors, according to Eq. (62). In the worst case, this implies a monolayer formation time of 1.4×10^7 sec/$(63)^2$ = 3500 sec (about 1 hour).

This estimate is somewhat pessimistic, since for these short times, the condition (59) is not satisfied, so that the full expression for $m(\psi)$, Eq. (57), should be used. In Figure 13, we show the $(c_0, \varkappa)$ parameter space: the curves shown correspond to the values of $(c_0, \varkappa)$ which satisfy the equality in Eq. (58), for a series of values for t_{mono} ranging from 4000 down to 2 hours. Also shown are the values of the $(c_0, \varkappa)$ parameters obtained from the fits to the photodesorption data (from Table 5).

Only data sets 1 and 5 (corresponding to OFHC copper) are close to satisfying the requirements for t_{mono} = 4000 hrs; the others would correspond to t_{mono} between 2 and 48 hrs. For the electrodeposited Cu data, a reduction in c_0 of from 1.2 to 1.8 orders of magnitude would be required to reach t_{mono} = 4000 hrs.

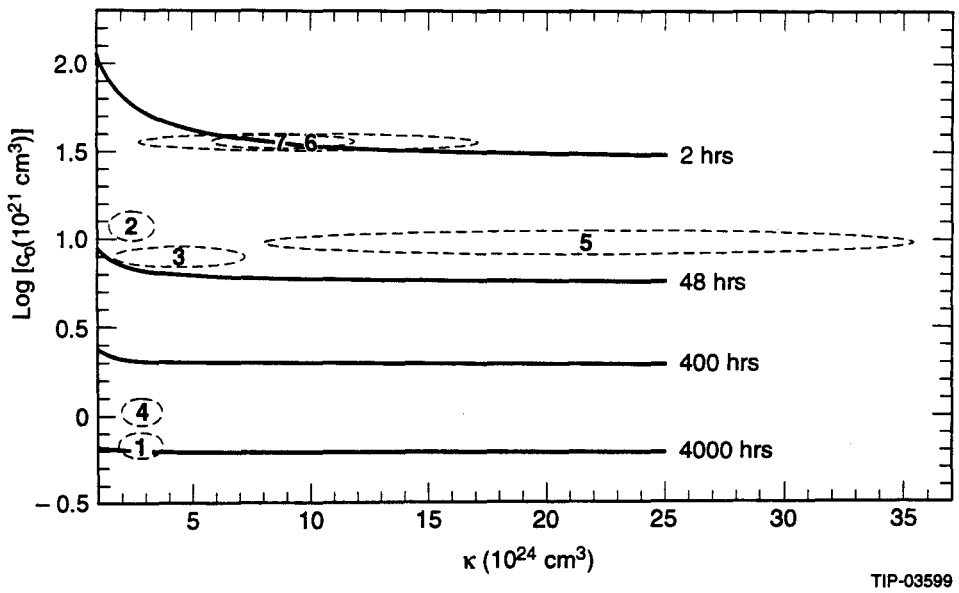

Figure 13. $(c_0, \varkappa)$ Parameter Space, Showing Curves of Constant t_{mono} (as Labeled) from Eq. (58), and the Data from Table 5. For $\dot{\gamma} = 10^{13}/\text{cm}^2/\text{sec}$.

5.1.2 Effect of Varying the Photon Flux

The flat regions for the curves in Figure 13 correspond to the region in which the asymptotic limit (Eq. (62)) is applicable: in this region, c_0 is independent of $\varkappa$. It is also true, in this region, that c_0 is independent of $\dot{\gamma}$. That is: *the monolayer formation time does not depend on the photon flux.*

The origin of this result can be seen simply as follows. The total gas evolved per unit area is given by

$$m(t) = \int_0^t \Phi(t')dt' = \dot{\gamma} \int_0^t \eta(t')dt' \quad . \tag{64}$$

Starting from Eq. (13), we have the following development:

$$\Phi(t) = D\frac{\partial c(0,t)}{\partial x} = \eta\dot{\gamma} \quad ,$$

$$\Phi(t) \cong D\frac{c_0}{\Delta x} \quad . \tag{65}$$

in which Δx is the region near the surface over which the concentration density varies from c_0 to a number close to zero,in the asymptotic limit (see Figure 8). This is the region over which the diffusion is primarily occurring, and the general relation between time and distance implicit in all solutions to the diffusion equation requires that

$$\Delta x \cong \sqrt{Dt} \tag{66}$$

where t is the time taken for the gradient $c_0/\Delta x$ to develop. Hence, substituting into Eq. (60), we obtain

$$\Phi(t) \cong \frac{c_0}{\sqrt{Dt}} \tag{67}$$

which shows that $\Phi(t)$, and hence $m(t)$, is independent of $\dot{\gamma}$. Physically, this arises because, as Eq. (65) shows, the gas flux leaving the surface in this model is determined entirely by that diffusing from the bulk, which depends only on the diffusion constant D, the concentration density c_0, and the time. This independence of Φ from $\dot{\gamma}$ also implies, from Eq. (65), that η varies inversely with $\dot{\gamma}$. This inverse dependence of η on $\dot{\gamma}$ is a fundamental prediction of the diffusion model and has been observed.[11]

The independence of $m(t)$ from $\dot{\gamma}$ breaks down when the asymptotic limit fails (for very small times or small values of $\dot{\gamma}$). However, even for photon fluxes equal to 1/100 that of the baseline SSC rate (10^{13}/cm^2/sec), the approximation of independence is reasonably good. This is shown in Figure 14, which is calculated from Eq. (58) and shows the $(c_0, \varkappa)$ parameter space, with curves of constant $t_{mono} = 4000$ hrs, for various values of $\dot{\gamma}$.

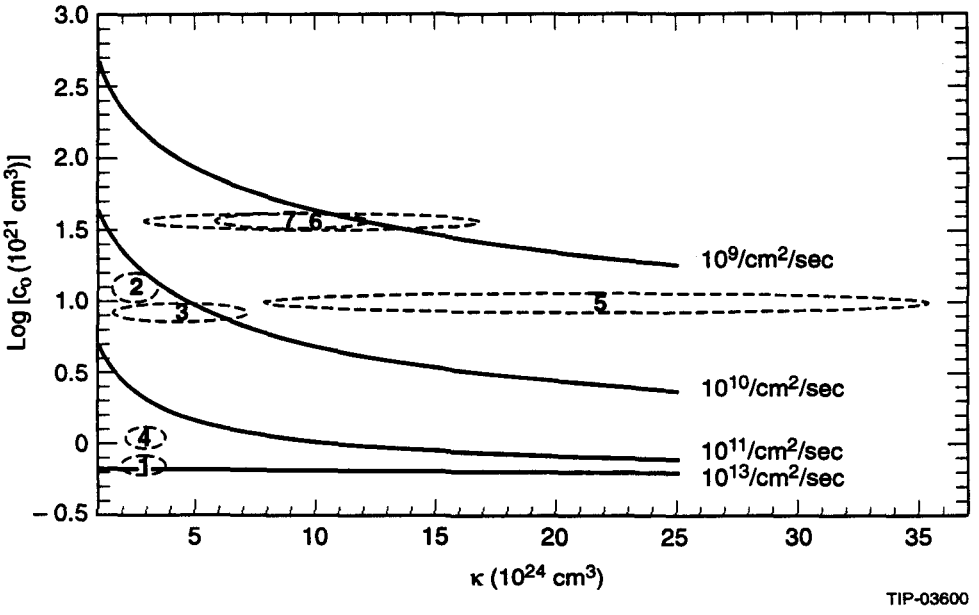

Figure 14. $(c_0, \varkappa)$ Parameter Space, Showing Curves of Constant $t_{mono} = 4000$ hrs, for Various Values of $\dot{\gamma}$ (As Labeled) from Eq. (58), Together with the Data from Table 5.

It is clear from Figure 14 that reduction of $\dot{\gamma}$ from the baseline rate by a factor of 100 results in only a small change in the value of c_0 required to achieve $t_{mono} = 4000$ hrs. In order to reach $t_{mono} = 4000$ hrs with the values of c_0 corresponding to the electrodeposited copper data, $\dot{\gamma}$ must be reduced to the range of 10^9–10^{10}/cm^2/sec, a factor of 10^3–10^4 below the baseline SSC value.

5.1.3 Effect of Varying the Diffusion Constant

Equation (62) indicates that the required value of c_0 varies inversely with the square root of D. The diffusion constant D has been taken in all the fits and calculations to be $D = 5 \times 10^{-18}$ cm^2/sec, which is a number appropriate to room temperature. This is correct for the data fits, since all the data analyzed has been taken at room temperature. However, for the situation we are considering for the SSC beam tube, the diffusion process is occurring in the metal or oxide film at 4 K. In general, the diffusion constant D may be expected to depend upon the temperature, at least linearly and more probably exponentially. In order to explore the sensitivity of the predictions of the diffusion model to this effect, the calculations have been repeated for a smaller value of D, equal to that scaled down from 5×10^{-18} cm^2/sec by the temperature ratio:

$$(4.2/300) \times 5 \times 10^{-18}\ \mathrm{cm}^2/\mathrm{sec} = 7 \times 10^{-20}\ \mathrm{cm}^2/\mathrm{sec}\ . \tag{68}$$

The results are shown in Figure 15.

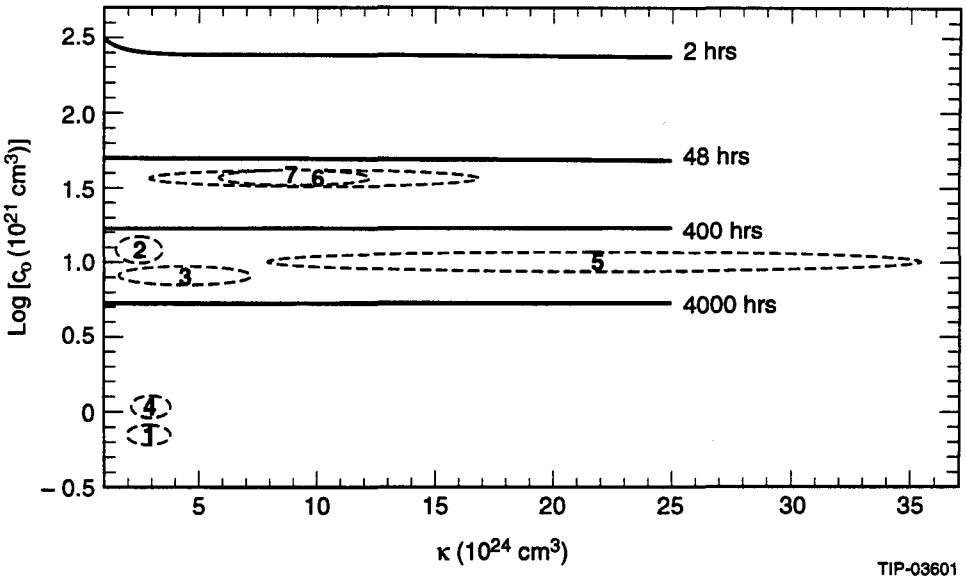

Figure 15. $(c_0, \varkappa)$ Parameter Space, Showing Curves of Constant t_{mono} (As Labeled) from Eq. (58), and the Data from Table 5. For $\dot{\gamma} = 10^{13}$/cm^2/sec, and for $D = 7 \times 10^{-20}$ cm^2/sec.

Since D is smaller, the requirements on c_0 are relaxed, as expected from Eq. (62). In this case, the electrodeposited copper data exceeds the required value of c_0 for $t_{mono} = 4000$ hours by only 0.25 to 0.85 orders of magnitude, a considerable improvement over the prediction of Figure 13.

Measurements[13] have been made of the photodesorption coefficient η for hydrogen at 4 K by the SSC-CDG. These measurements found virtually no difference in the room temperature coefficient and the 4 K coefficient. The diffusion model, with the diffusion constant varying linearly with temperature as assumed above, would predict roughly an order of magnitude smaller coefficient at 4 K, which was clearly not seen in the data. However, it is noted in Reference 13 that the cold measurements were done for surfaces which had become coated with about 0.1 monolayers of H_2 from extraneous sources. Data from Reference 5 indicates that photodesorption from cold surfaces coated with "physisorbed" H_2 is enhanced due to the presence of this hydrogen by factors of about 300 times the fractional monolayer coverage of the physisorbed hydrogen. In this case, then, one might expect a 30 × enhancement factor due to the 0.1 monolayers of physisorbed hydrogen, which could explain the observed rough equality between the cold and warm photodesorption measurements.

5.2 $r > 0$

5.2.1 Estimate of Required c_0

We now discuss the case of finite r. In this case, the equation which defines the acceptable range of parameter space is Eq. (57). Again, we may consider the applicability of the asymptotic limit, which would correspond to the limit in Eq. (55). In this case, not only do we have the requirement cited in Eq. (60), but we also require that $r\psi_{\text{mono}} \gg 1$, which implies;

$$t_{\text{mono}} \gg \tau_p = \frac{1}{\Lambda^2 D} \quad , \tag{69}$$

$$\frac{1}{\Lambda} \ll \left[\frac{1}{\Lambda}\right]_{\text{max}} = \sqrt{D t_{\text{mono}}} \quad . \tag{70}$$

Using $t_{\text{mono}} = 1.4 \times 10^7$ sec and $D = 5 \times 10^{-18}$ cm^2/sec we obtain $(1/\Lambda)_{\text{max}} = 836$ Å. The values of $1/\Lambda$ found from the fits to the data, as given in Table 6a, are smaller than $(1/\Lambda)_{\text{max}}$, but not by very much. Thus, we may expect that the asymptotic form will not be very useful. Nevertheless, it is instructive to examine it. The analog of Eq. (61) is

$$m(\psi_{\text{mono}}) = \frac{c_0 D}{\varkappa \dot{\gamma}} \left[\frac{1}{\sqrt{r}} - \frac{\left(1 + \sqrt{r}\right)}{r\sqrt{\pi \psi_{\text{mono}}}}\right] \leq m_0 \quad . \tag{71}$$

Substituting $\psi_{\text{mono}} = t_{\text{mono}}/\tau$, and using Eq. (20) for τ and Eq. (44) for r, we obtain the following relation:

$$c_0 \leq \frac{m_0 \Lambda}{1 - \sqrt{\frac{D}{[\varkappa\dot{\gamma}]^2 \pi t_{\text{mono}}}} - \sqrt{\frac{1}{\Lambda^2 \pi t_{\text{mono}} D}}} \quad . \tag{72}$$

The condition which obtains in the limit $t_{\text{mono}} \rightarrow \infty$ is just $c_0 < m_0\Lambda$, that is, that the total gas load is less than 1 monolayer. Corrections to this for finite t_{mono} are represented by the two square-root terms in the denominator. However, this form is not very useful because the requirements of Eqs. (59) and (69), under which the asymptotic limit is obtained, require that each of these square-root terms be small compared to 1. Hence this form is only appropriate to evaluate small corrections to the limit $c_0 < m_0\Lambda$.

We must refer to the complete expression, Eq. (57), in general. In Figure 16, we show the (c_0, Λ) parameter space: the curves shown correspond to the values of (c_0, Λ) which satisfy the equality in Eq. (57), for a series of values for t_{mono} ranging from 4000 down to 2 hours. The solid curves correspond to $\varkappa = 10^{-24}$ cm^3; the dotted curves correspond to $\varkappa = 10^{-23}$ cm^3. Also shown are the values of the (c_0, Λ) parameters obtained from the fits to the photodesorption data (from Table 6).

Again, only data set 1 (OHFC copper) is close to satisfying the requirements for $t_{\text{mono}} = 4000$ hrs; the others would correspond to t_{mono} between 2 and 48 hrs. However, for the electrodeposited Cu data, the reduction in c_0 required to reach $t_{\text{mono}} = 4000$ hrs is now seen to be smaller than in the analysis with $r = 0$: it ranges from 0.8–1.3 orders of magnitude.

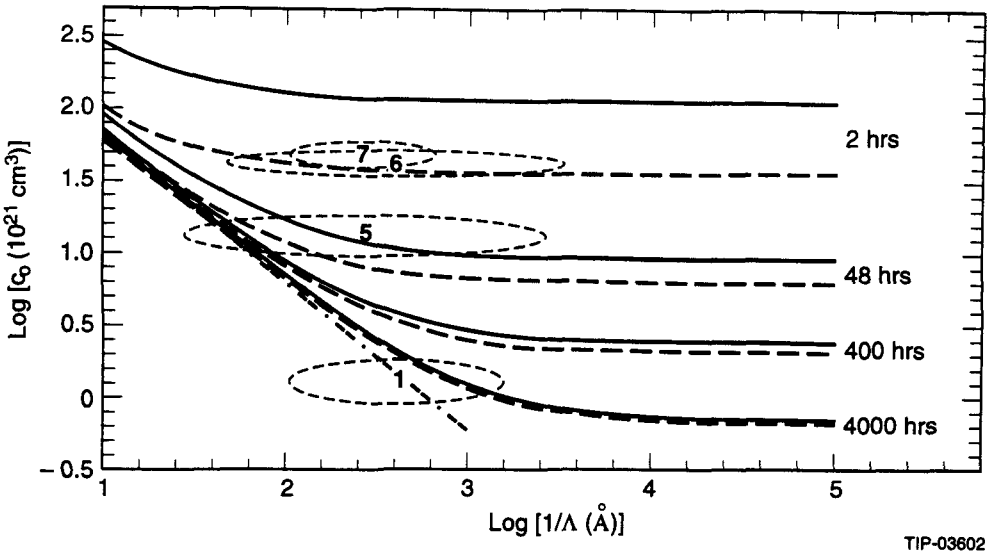

Figure 16. (c_0, Λ) Parameter Space, Showing Curves of Constant t_{mono}, (As Labeled) from Eq. (57), and the Data from Tables 6a and 6b. The solid curves correspond to $\varkappa = 10^{-24}$ cm^3; the dotted curves correspond to $\varkappa = 10^{-23}$ cm^3. The dot-dash line represents the asymptotic limit $c_0 = m_0\Lambda$. The curves have been calculated for $\dot{\gamma} = 10^{13}$/cm^2/sec.

5.2.2 Effect of Varying the Photon Flux

Again, we may look at the dependence on $\dot{\gamma}$ for this case. This is shown in Figure 17. This figure shows the (c_0, Λ) parameter space, with curves of constant $t_{mono} = 4000$ hrs, for various values of $\dot{\gamma}$.

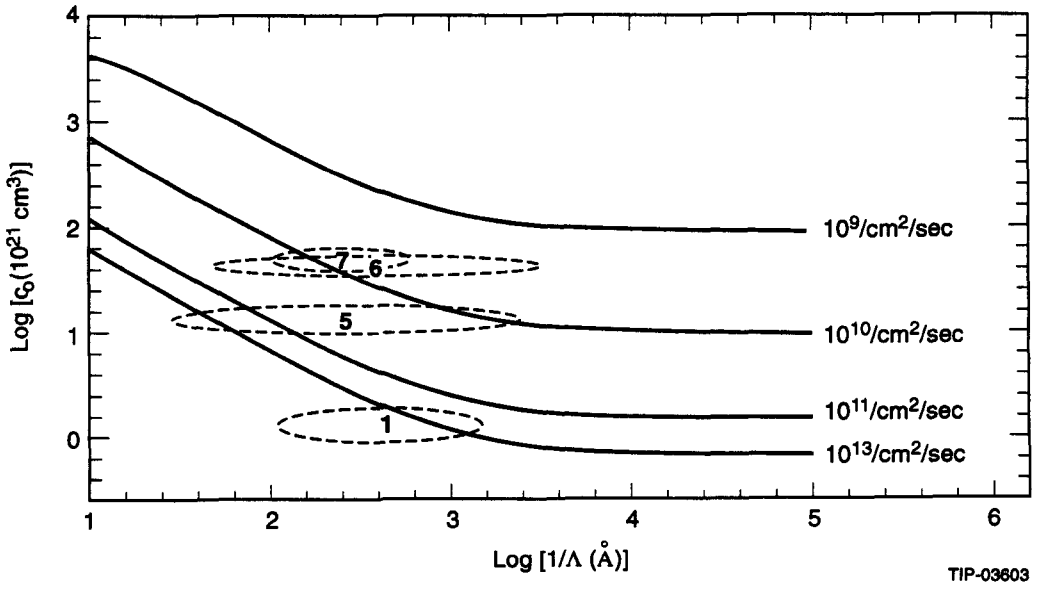

Figure 17. (c_0, Λ) Parameter Space, Showing Curves of Constant $t_{mono} = 4000$ hrs, from Eq. (57), and the Data from Tables 6a and 6b. The curves are labeled by the corresponding valued of $\dot{\gamma}$. $\varkappa$ has been fixed at 5×10^{-24} cm^3.

In this case, $\dot{\gamma}$ would need to be reduced to about 10^{10}/cm^2/sec in order to reach $t_{mono} = 4000$ hrs for the worst-case electrodeposited copper beam tube data.

5.2.3 Effect of Varying the Diffusion Constant

The effect of a reduced D is shown in Figure 18. As was the case for $r = 0$, there is a substantial improvement in the value of c_0 required, although the improvement is not as great as in the case of $r = 0$. This is not unreasonable: the smaller D slows down the diffusion process, so that the advantage of a finite gas load is reduced. The worst-case data fails for $t_{mono} = 4000$ hrs by about 0.8 orders of magnitude.

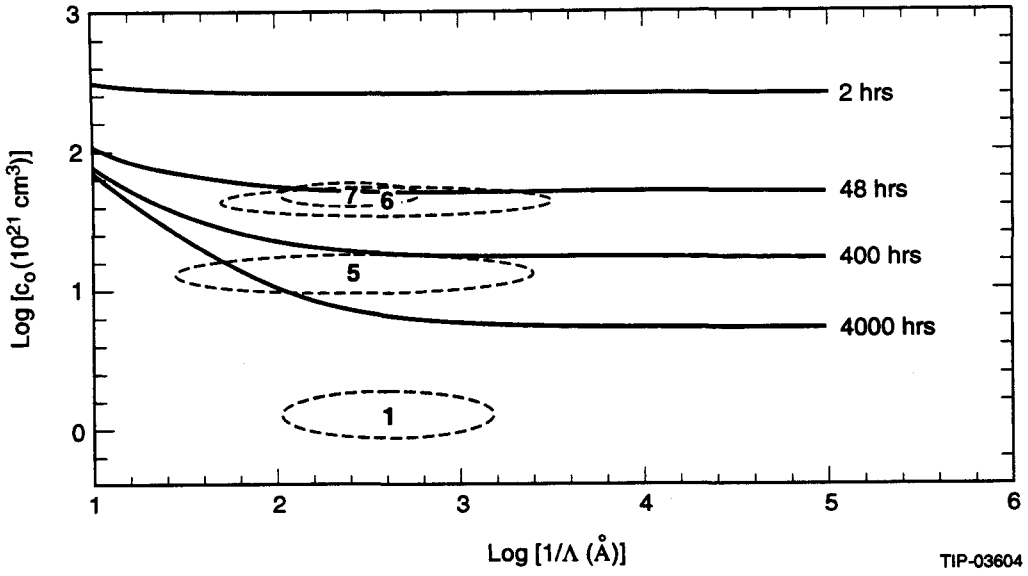

Figure 18. (c_0, Λ) Parameter Space, Showing Curves of Constant t_{mono} (As Labeled) from Eq. (57), and the Data from Tables 6a and 6b. The curves correspond to $\varkappa = 5 \times 10^{-24}$ cm^3, $D = 7 \times 10^{-20}$ cm^2/sec, and $\dot{\gamma} = 10^{-13}$ cm^2/sec.

5.3 Estimates of the Effect of a Magnetic Field

It is generally believed[14] that the liberation of gas in the photodesorption process is mediated by low energy photoelectrons. The photons produce slow (few tens to a hundreds of eV) electrons through the photoelectric effect; these photoelectrons, in turn, liberate gas molecules through electrodesorption. This two-step mechanism is believed to dominate over the direct ejection of gas molecules via photon-molecule interactions.

In a closed tube, such as a beam tube, the photoelectrons would in general be ejected such that they electrodesorb the whole inside surface of the tube, relatively independent of the point on the tube at which the photons are incident. Thus, the assumption of uniform desorption from the entire inside diameter of the tube, as has been made in the analysis above, is appropriate, even though the photon beams typically are tightly collimated and illuminate only a narrow strip a few millimeters high along the length of the beam tube.

The situation is altered significantly, however, in the presence of a magnetic field transverse to the axis of the beam tube. If this field is sufficiently strong that the cyclotron radius of hundred-eV electrons is less than a few millimeters, then all the photoelectrons produced by a narrowly collimated photon beam will be confined to the region of the tube's surface which the photon beam illuminates, and will electrodesorb this area only. In this case, the effective flux will be quite high over this area,and zero elsewhere. This area will clean up rapidly. Other areas of the beam tube will only liberate gas due to photons scattered from the directly illuminated area. These other areas will clean up more slowly. The net result will be an "average" photodesorption coefficient which has a more complicated dependence on time than in the simple diffusion model.

This process can be modeled in the following way. Let s designate the circumferential distance inside the tube which is directly illuminated by the photon beam; then the rest of the tube's inside surface is $\pi d - s$, where d is the tube inside diameter. Let ϱ designate the fraction of the photons which are reflected upon direct illumination. We assume that these photons are reflected such that they are uniformly distributed around the rest of the tube's inner diameter. With these assumptions, we can write for $\dot{\gamma}_1$, the photon flux associated with the directly illuminated surface s (surface 1),

$$\dot{\gamma}_1 = (1 - \varrho)\frac{\dot{N}_\gamma}{s} = (1 - \varrho)\frac{\dot{\gamma}}{\delta} = \sigma_1\dot{\gamma} \tag{73}$$

where $\dot{N}_\gamma$ is the photon flux per linear centimeter, $\dot{\gamma} = \dot{N}_\gamma / \pi d$ is the "average" value of the photon flux (defined as in the earlier sections above), $\delta = s/d$, and $\sigma_1 = (1-\varrho)/\delta$. Similarly, for $\dot{\gamma}_2$, the photon flux on the indirectly illuminated surface (surface 2) due to reflections from the directly illuminated region, we have

$$\dot{\gamma}_2 = \varrho\frac{\dot{N}_\gamma}{\pi d - s} = \varrho\frac{\dot{\gamma}}{1 - \delta} = \sigma_2\dot{\gamma} \tag{74}$$

with $\sigma_2 = \varrho\ (1-\delta)$. The photodesorption coefficient for surface i ($i = 1,2$) is

$$\eta_i = \varkappa c_0 y(\psi_i)\ ,$$

$$y(x) = \mathrm{Exp}(x)\mathrm{Erfc}\left(\sqrt{x}\right) \tag{75}$$

where

$$\psi_i = \frac{t}{\tau_i} = \frac{t\left(\varkappa\dot{\gamma}_i\right)^2}{D}$$

$$= \sigma_i^2\psi\ . \tag{76}$$

The gas per unit time, per unit length along the tube, evolved from surfaces 1 and 2 is then

$$\dot{g}_1 = s\dot{\gamma}_1\eta_1\ ;$$

$$\dot{g}_2 = (\pi d - s)\dot{\gamma}_2\eta_2\ . \tag{77}$$

The "average" photodesorption coefficient can then be written as

$$\eta(\psi) = \frac{(\dot{g}_1 + \dot{g}_2)}{\pi d \dot{\gamma}}$$

$$= \delta\sigma_1\eta_1 + (1 - \delta)\sigma_2\eta_2 \ ,$$

$$\frac{\eta(\psi)}{\varkappa c_0} = (1 - \varrho)y(\sigma_1{}^2\psi) + \varrho y(\sigma_2{}^2\psi) \ . \tag{78}$$

The first term in this expression represents the contribution from the directly illuminated surface, which cleans up rapidly (since typically $\delta \ll 1$ so $\sigma_1 \gg 1$). The second term represents the contribution from the indirectly illuminated surface, which cleans up slowly (if ϱ is small, since σ_2 is proportional to ϱ), and which is suppressed by the factor ϱ. We recover the original expression for $\eta(\psi)$ when $\varrho = 1-\delta$.

The expression for η is plotted in Figure 19, for various values of ϱ, to illustrate the transition from the fast cleanup to slow cleanup terms. The value of δ has been taken as representative of that in the SSC situation: $s = 4$ mm, $d = 33$ mm, so $\delta = 3.8\%$.

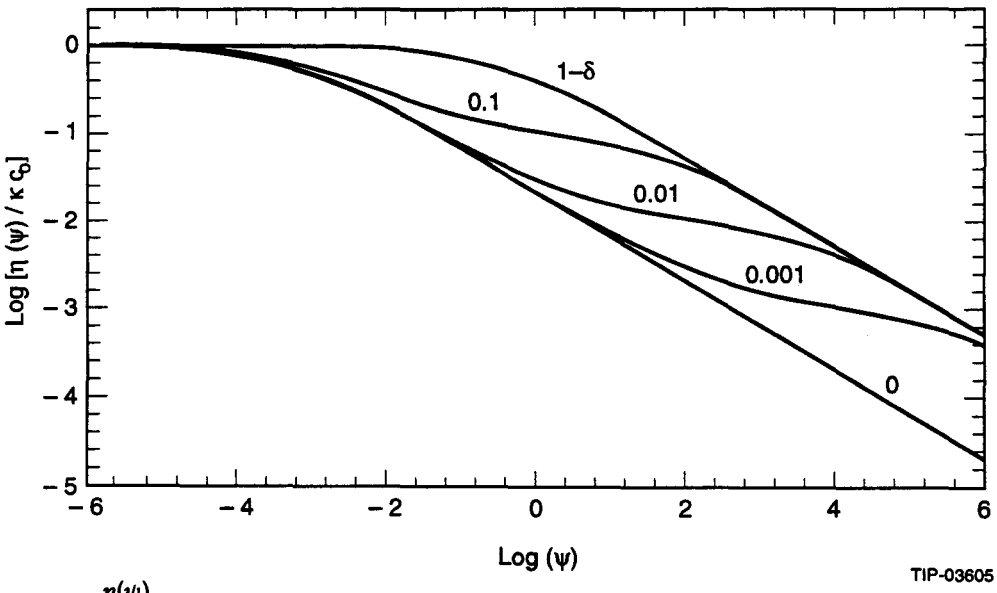

Figure 19. $\frac{\eta(\psi)}{\varkappa c_0}$, from Eq. (78), vs. ψ, for Several Values of ϱ (As Labeled). Calculated for $\delta = 0.038$.

This modification of the effective photodesorption coefficient will clearly have some impact on the monolayer formation time. A rough feeling for the impact can be obtained by writing down the expression relating the effective photodesorption coefficient to the total gas evolved, and examining it in the asymptotic limit. Using Eqs. (78) , we have that

$$m(t) = \frac{1}{\pi d}\int_0^t \left[\dot{g}_1(t') + \dot{g}_2(t')\right] dt' \ ,$$

$$m(t) = \dot{\gamma}\varkappa c_0 \int_0^{\psi(t)} \left[(1-\varrho)y(\sigma_1{}^2\psi')\tau_1 + \varrho y(\sigma_2{}^2\psi')\tau_2\right] d\psi' \ ,$$

$$\frac{m(\psi)}{\left[\frac{c_0 D}{\varkappa\dot{\gamma}}\right]} = \int_0^{\psi} \left[\frac{(1-\varrho)}{\sigma_1{}^2} y\left(\sigma_1{}^2\psi'\right) + \frac{\varrho}{\sigma_2{}^2} y\left(\sigma_2{}^2\psi'\right)\right] d\psi' \ . \tag{79}$$

The results of doing the integral are given in Eq. (47). In the asymptotic limit, $\sigma_1{}^2\psi \gg 1$ and $\sigma_2{}^2\psi \gg$ (which, for small δ and ϱ, amounts to the requirement that $\varrho^2\psi \gg 1$), we have, using Eq. (54),

$$\frac{m(\psi)}{\left[\frac{c_0 D}{\varkappa\dot{\gamma}}\right]} \to 2\sqrt{\frac{\psi}{\pi}} \left[\frac{(1-\varrho)}{\sigma_1} + \frac{\varrho}{\sigma_2}\right]$$

$$\to 2\sqrt{\frac{\psi}{\pi}} \ . \tag{80}$$

In the asymptotic limit, the total gas evolved from the surface, per unit area, is thus independent of ϱ and δ. This result is not surprising, given the fact that this quantity, in the asymptotic limit, was shown in the previous section to be independent of the photon flux.

We may thus expect that the monolayer formation time will not be very dependent upon ϱ or δ, except for very small ϱ, for which the asymptotic limit $\varrho^2\psi \gg 1$ is not reached. In this case, the equation relating the parameters of the problem to the monolayer formation time is derived by integrating Eq. (79); the result, in a form analogous to Eq. (58), is

$$\frac{c_0 D}{\varkappa\dot{\gamma}} \left[\begin{array}{l} \frac{(1-\varrho)}{\sigma_1{}^2}\left[2\sqrt{\frac{\sigma_1{}^2\psi_{\text{mono}}}{\pi}} - 1 + \text{Exp}\left(\sigma_1{}^2\psi_{\text{mono}}\right)\text{Erfc}\left(\sqrt{\sigma_1{}^2\psi_{\text{mono}}}\right)\right] + \\ \frac{\varrho}{\sigma_2{}^2}\left[2\sqrt{\frac{\sigma_2{}^2\psi_{\text{mono}}}{\pi}} - 1 + \text{Exp}\left(\sigma_2{}^2\psi_{\text{mono}}\right)\text{Erfc}\left(\sqrt{\sigma_2{}^2\psi_{\text{mono}}}\right)\right] \end{array}\right] \leq m_0 \tag{81}$$

The values of the parameters (c_0, $\varkappa$) which satisfy the equality are shown in Figure 20, for a fixed $t_{\text{mono}} = 4000$ hrs, and for various values of ϱ.

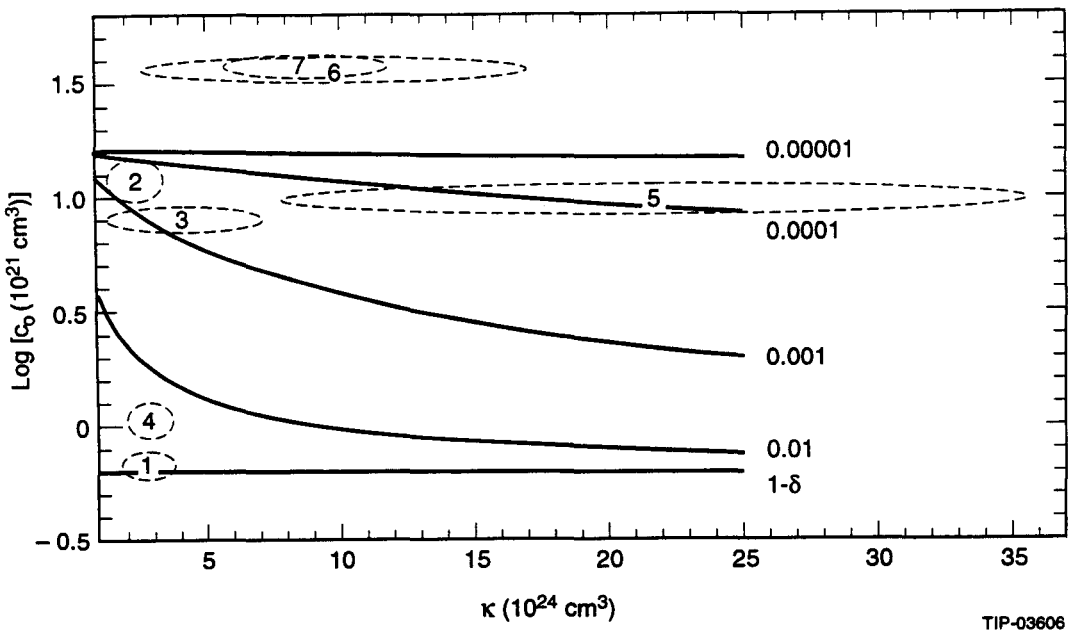

Figure 20. $(c_0, \varkappa)$ Parameter Space, Showing Curves of Constant ϱ (As Labeled), for t_{mono} = 4000 hrs. From Eq. (81); data from Table 5. For $\dot{\gamma} = 10^{13}$/cm^2/sec, and $\delta = 0.038$.

Very little change is seen for $\varrho > 0.01$, except for small $\varkappa$. Values of the reflectivity ϱ in the range of 0.0001 or lower are required to reach the electrodeposited copper data sets. This would require >99.99% of the photons to be absorbed in the directly illuminated area. Measurements[15] of ϱ from an unpolished electrodeposited copper surface at incidence angles of 1° have obtained values of ϱ of 2×10^{-3} for 120 eV photons. The incidence angle at the SSC will be about 0.1°. It seems unlikely that values of ϱ in the range of 10^{-4} can be achieved.

We can also extend this model to the case of finite r. The equation analogous to Eq. (81), for finite r, is

$$\frac{c_0 D}{\varkappa \dot{\gamma}} \left[\frac{(1-\varrho)}{\sigma_1^2} \left[\frac{\sigma_1}{\sqrt{r}} - \frac{\mathrm{Exp}(\sigma_1^2 \psi_{mono})\mathrm{Erfc}\left(\sqrt{\sigma_1^2 \psi_{mono}}\right) - \frac{\sigma_1 \mathrm{Exp}(r\psi_{mono})\mathrm{Erfc}(\sqrt{r\psi_{mono}})}{\sqrt{r}}}{\frac{\sqrt{r}}{\sigma_1} - 1} \right] + \frac{\varrho}{\sigma_2^2} \left[\frac{\sigma_2}{\sqrt{r}} - \frac{\mathrm{Exp}(\sigma_2^2 \psi_{mono})\mathrm{Erfc}\left(\sqrt{\sigma_2^2 \psi_{mono}}\right) - \frac{\sigma_2 \mathrm{Exp}(r\psi_{mono})\mathrm{Erfc}(\sqrt{r\psi_{mono}})}{\sqrt{r}}}{\frac{\sqrt{r}}{\sigma_2} - 1} \right] \right] \leq m_0 \ . \qquad (82)$$

In Figure 21, the (c_0, Λ) parameter space is shown: the curves correspond to the values of c_0 and Λ which satisfy the equality in Eq. (82), for fixed values of t_{mono} = 4000 hrs, and for $\varkappa = 5 \times 10^{-24}$ cm^3 and $\delta = 0.038$.

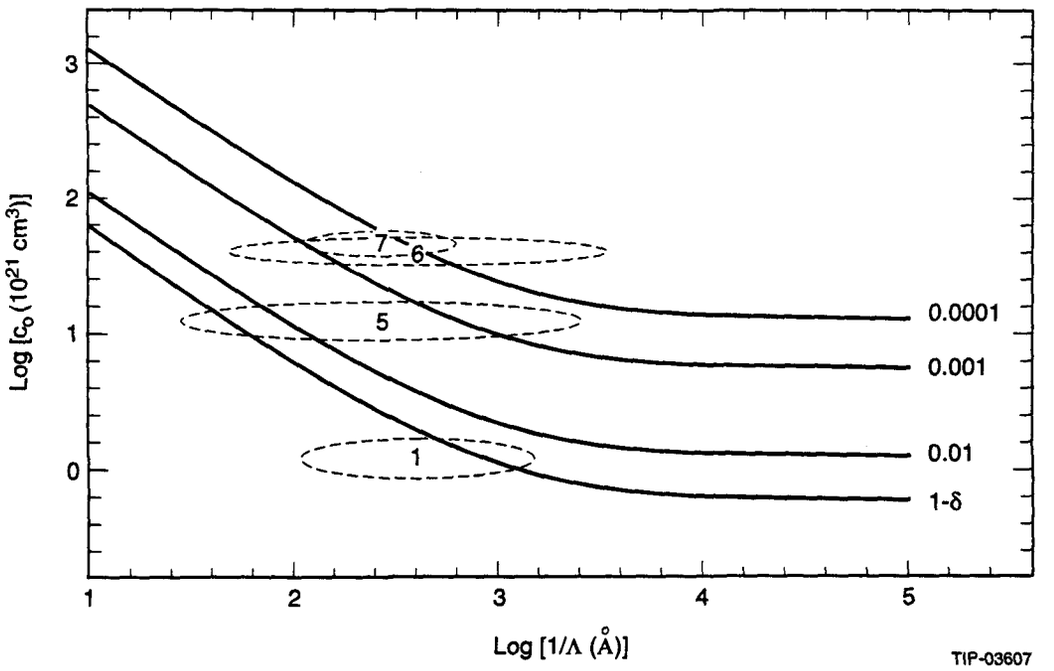

Figure 21. (c_0,Λ) Parameter Space, Showing Curves of Constant t_{mono} = 4000 hrs, from Eq. (82), and the Data from Table 6. The curves are labeled by the corresponding values of ϱ. $\varkappa$ has been fixed at 5 × 10^{-24} cm^3, δ = 0.038, and $\dot{\gamma}$ = 10^{13}/cm^2/sec.

In this case, we see that values of ϱ at the level of a few parts per thousand would be satisfactory for data set 5, although another order of magnitude would be required if the surface had the parameters of data sets 6 or 7.

6.0 CONCLUSIONS

A diffusion model has been applied to analyze hydrogen photodesorption data from a number of surfaces which may be useful as candidates for the inside diameter of the SSC beam tube. The model has been used to extract semi-phenomenological parameters from the data, which are related to the hydrogen volume concentration in the metal (or surface oxide), the effective cross section for photodesorption, and the finite total gas load in the metal.

The model has then been applied to the SSC situation in order to make estimates of the time required to desorb a monolayer of hydrogen. Sensitivity of the estimates to the details of the model, the photon flux rate, possible dependences of the diffusion constant on temperature, and the possible effects of a magnetic field, have been explored.

A summary of the results is given in Tables 7a and 7b. We choose to focus on data set 6 only, as representative of the baseline SSC electrodeposited copper beam tube surface. In Tables 7a and 7b, we present the change in the parameters of the surface ($c0$,Λ, D or ϱ) or in the photon flux $\dot{\gamma}$, which, *considered by itself*, is required to reach t_{mono} = 4000 hours. As the detailed discussion above has shown, none of these changes are related each other or to t_{mono} in a linear fashion. Any combination of changes must be studied specifically using the tools developed above.

TABLE 7A. FOR THE 2-PARAMETER (r = 0) MODEL.

PARAMETER	CHANGE REQUIRED TO REACH t_{mono} = 4000 HRS
Concentration Density at the Surface c_0	Factor of 63 Reduction
Photon Flux $\dot{\gamma}$	Factor of 10^4 Reduction
Diffusion Constant: D	Factor of 4000 Reduction
Surface Reflectivity ϱ	$<< 10^{-5}$

TABLE 7B. FOR THE 3-PARAMETER (r = 0) MODEL.

PARAMETER	CHANGE REQUIRED TO REACH t_{mono} = 4000 HRS
Concentration Density at the Surface c_0	Factor of 22 Reduction
Concentration Density Mean Depth: $(1/\Lambda)$	Factor of 25 Reduction
Photon Flux $\dot{\gamma}$	Factor of 2000 Reduction
Diffusion Constant: D	Factor of 4000 Reduction
Surface Reflectivity ϱ	$< 10^{-4}$

REFERENCES

1. M. Andritschky, O. Grobner, A. G. Mathewson, F. Schumann, P. Strubin, R. Souchet, "Synchrotron Radiation Induced Neutral Gas Desorption from Samples of Vacuum Chambers," *Vacuum*, **38**, 8, 933, (1988).
2. M. D. Malev, "Gas Absorption and Outgassing of Metals," *Vacuum*, **23**, 2, 43(1972).
3. J. Crank, *The Mathematics of Diffusion*, 2nd edition,32–38, Oxford Science Publications, (1975).
4. Data presented by O. Grobner at the *Nov 13, 1992 SSCL Vacuum Workshop*.
5. D. Bintinger, P. Limon, H. Jostlein, D. Trbojevic, "Status of the SSC Photodesorption Experiment," *SSC-102,* 1986.
6. C. Forester, H. Halama, C. Lanni, "Photon-Stimulated Desorption Yields from Stainless Steel and Copper-plated Beam Tubes with Various Pretreatments," *J. Vac Sci Technol* **A8(3)**, 2856 (1990).
7. A. G. Mathewson, O. Grobner, P. Strubin, P. Marin, R. Souchet,"Comparison of Synchrotron Radiation Induced Gas Desorption from Al, Stainless Steel and Copper Chambers," *Proc of the Conference on the Vacuum Design of Synchrotron Light Sources*, Argonne, (1990).
8. Unpublished data from BINP/SSCL measurements, data set #0002.
9. Unpublished data from BINP/SSCL measurements, data set #0009.
10. Unpublished data from BNL/SSCL measurements, data set #0024.
11. M. Andritschky, O. Grobner, A. G. Mathewson, P. Strubin, R.Souchet, B. Trickett, "Differences in Synchrotron Radiation Induced Gas Desorption from Stainless Steel and Aluminum Alloy," *Proc. of the 1989 Particle Accelerator Conference*, 563, Chicago, (1989).
12. M. Andritschky, "Damage of Oxide Layers on an Al-alloy by Electron Bombardment," *Vacuum*, **39, 7**, 649, (1989).
13. D. Bintinger, P. Limon, R. Rosenberg, "Photodesorption from Copper-plated Stainless Steel at Liquid Helium Temperature and Room Temperature," *J. Vac. Sci. Technol*, **A7(1)**, 59, (1989).
14. O. Grobner, A. G. Mathewson, P. Strubin, E. Algae, R. Souchet, "Neutral Gas Desorption and Photoelectric Emission from Aluminum Alloy Vacuum Chambers Exposed to Synchrotron Radiation," *J. Vac. Sci. Technol*, **A7(2)**, 223, (1989).
15. Data presented by P. Lippel at the *Nov 13, 1992 SSCL Vacuum Workshop*.